



Exploring Study of Magnetic and Electrical Properties of Tl^{3+} Doped $Co_{0.5}Ni_{0.5}Fe_2O_4$ Spinel Ferrites

Touseef Ahmad¹, M.U. Islam^{1*}, I.H Gul², Mutawara Mahmood Baig³, M. Ajmal¹

¹ Institute of Physics, Bahauddin Zakariya University, Multan, Pakistan

² School of Chemical & Materials Engineering (SCME), NUST, Islamabad, Pakistan

³ School of Chemistry and Chemical Engineering, Yangzhou University, Yangzhou, Jiangsu, 225009 P. R. China

ARTICLE INFO

Article History:

Received: February 26, 2023

Revised: April 29, 2023

Accepted: May 06, 2023

Available Online: June 28, 2023

Keywords:

Sol-Gel Auto Combustion

Spinel Ferrites

X-Ray Diffraction

Magnetic Susceptibility

Dielectric Properties

Resistivity

ABSTRACT

$Co_{0.5}Ni_{0.5}Fe_{2-x}Tl_xO_4$ ($x=0, 0.05, 0.1, 0.15,$ and 0.2) spinel ferrites were prepared via the sol-gel technique. The XRD analysis revealed a single-phase spinel structure. The lattice constant 'a' increased from 8.223-8.269Å with doping of Tl^{+3} due to larger ionic radii of Tl^{+3} than Fe^{+3} ions. The mass susceptibility at 300K decreased from 7.46×10^{-3} - 4.15×10^{-3} cm³/g due to the weakening of AB interactions followed by a decrease in Curie temperature from 453K to 408K. The electrical permittivity follows the Maxwell-Wagner model and Koop's theory. The dc resistivity of ferrites at 300K increased from 1.82×10^9 - 9.23×10^9 Ω-cm with increasing Tl^{+3} contents due to increased hopping lengths. The activation energy obtained from Arrhenius plots increased from 0.126 to 0.131eV, increasing Tl^{+3} contents.

OPEN ACCESS

© 2023 The Authors, Published by iRASD. This is an Open Access article under the Creative Commons Attribution Non-Commercial 4.0

*Corresponding Author's Email: dr.misbahulislam@bzu.edu.pk

1. Introduction

Spinel ferrites have got prime importance due to their versatile properties. These magnetic materials have high resistivity (Goldman, 2006; Jalaiah, Mouli, Krishnaiah, Babu, & Rao, 2019) and low eddy current losses. The nanoparticles of spinel ferrites exhibit novel properties that are useful in biomedical applications. Spinel ferrites are low-cost and easy to fabricate for various engineering applications like recording media, microwave absorbers, sensors, etc (Kazimierczuk, 2009). Amongst the various methods available for the preparation of sol-gel technique is low cost and easy to handle. The homogeneous distribution of nanoparticles is obtained using the sol-gel method (Battoo, Kumar, & Lee, 2009; Cullity & Graham, 2011). Co-Ni spinel ferrites have attracted the attention of materials scientists (Abdel-Latif, 2012; Abdul-Aziz, Abraham, & Khaleel, 2013; Asghar et al., 2018; Singha, Singhb, & Dosanjha, 2015; Velhal, Patil, Shelke, Deshpande, & Puri, 2015) due to high saturation magnetization and Curie temperature. Since Co is more anisotropic (Kambale, Shaikh, Kamble, & Kolekar, 2009; Ortiz-Quifonez, Pal, & Villanueva, 2018) compared to Ni, Co-Ni spinel ferrites become superior to other spinels. The substitution of transition metal ions in the Co-Ni ferrites may augment the magnetic properties.

Velhal *et al.* (Velhal et al., 2015) reported the Ni-doped Co spinel ferrites via low-temperature auto-combustion technique and reported that increasing the Ni content in Cobalt ferrite decreases the magnetization because of the lower magnetic moment of nickel than cobalt. Gaffoor *et al.* (Gaffour & Ravinder, 2014) synthesized the Co-doped $NiFe_2O_4$ spinel ferrites by the sol-gel route. They reported that increasing the Cobalt content in $NiFe_2O_4$ increases the lattice parameter and crystallite size. Amirabadizadeh *et al.* (Amirabadizadeh & Amirabadi, 2013) synthesized the Al-doped $Ni_{0.6}Co_{0.4}Fe_2O_4$ spinel ferrites via the sol-gel route. They reported that by increasing the content of Al^{+3} (0-0.7) in

Ni-Co spinel ferrites, the crystallite size decreases from 29nm to 10nm. Similarly, the saturation magnetization decreases from 61-10 emu/g with increasing Al⁺³ content in Ni-Co spinel ferrites. Farid *et al.* (M. Farid et al., 2015) reported the effect of Nd on the electrical properties of Ni-Co spinel ferrites prepared by the sol-gel route and observed that both the dc resistivity and activation energy increase with Nd doping in Ni-Co spinel ferrites.

In the present work, Tl-substituted Co_{0.5}Ni_{0.5}Fe₂O₄ ferrites are prepared by the sol-gel technique. To the best of our knowledge, the Tl-doped Co-Ni spinel ferrites have yet to be reported frequently in the literature. There was a need to investigate the Tl-doped Co-Ni ferrites.

2. Experimental Procedure

Thallium (Tl) doped Co_{0.5}Ni_{0.5}Fe₂O₄ spinel ferrites were prepared via the sol-gel auto-combustion method. Analytical grade starting materials were used; Fe(NO₃)₃.9H₂O, TlNO₃, Ni(NO₃)₃.6H₂O, Co(NO₃)₃.6H₂O, and citric acid. Stock solutions of all the nitrate salts and citric acid were prepared in 100 mL of distilled water in a beaker. These stock solutions were added to a 1000 mL beaker and stirred at 70°C continuously to obtain a homogeneous solution. Ammonium hydroxide was added dropwise in the solution to maintain the pH = 7. After complete evaporation, a thick gel is formed; stirring was stopped, and the gel was burnt at about 400°C by the auto combustion process. The complete combustion of the ash gives ferrite powder (be implemented from June; Kumar et al., 2015; Sajjadi, 2005). The ash was ground and sintered at 1050°C for 5 hours in a box furnace. The following Fig. (1) shows the steps for the sol-gel method.

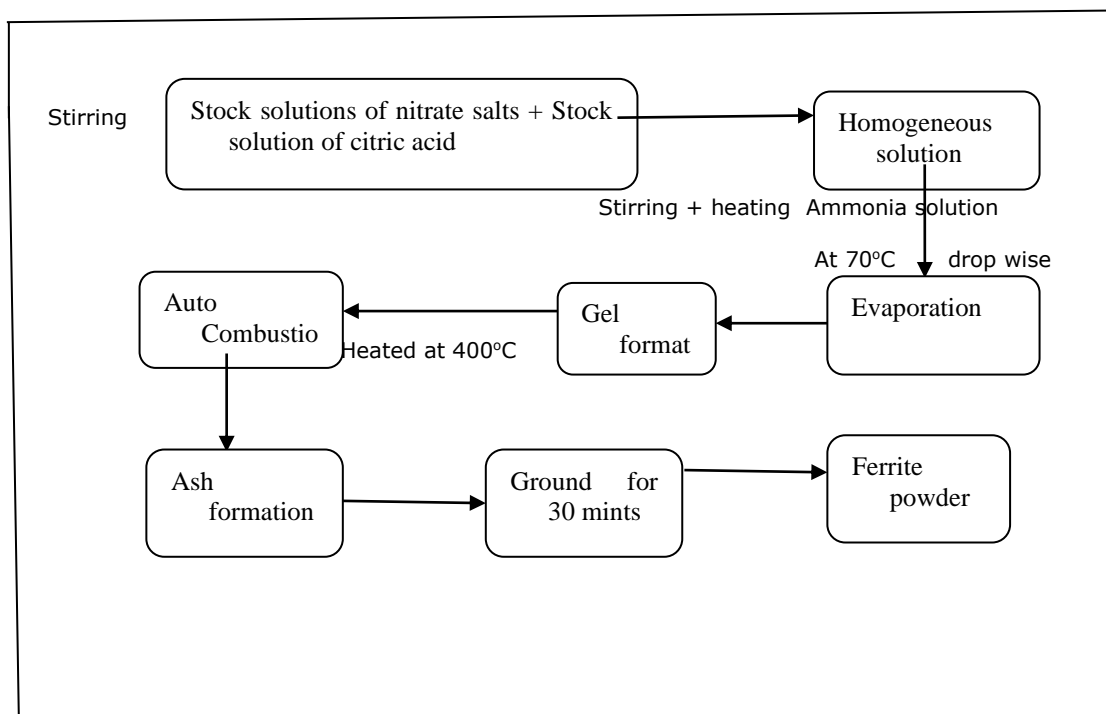


Figure 1: Flow chart of sol-gel process

2.1. Characterizations Techniques

2.1.1. X-ray Diffraction

X-ray diffraction is used to determine the phase purity of samples; d-values, lattice constant, and hopping length may be determined from XRD data. Bragg's law is used to determine the d-values of a specimen. Bragg's law is given below (de Almeida et al.; Suryanarayana, Norton, Suryanarayana, & Norton, 1998):

$$2d\sin\theta = n\lambda \quad (1)$$

Where θ is the Bragg angle, and d is the inter-planer spacing. The lattice constant is determined by using the following equation (Kumar et al., 2015):

$$a = \frac{\lambda}{2\sin\theta} \sqrt{h^2 + k^2 + l^2} \quad (2)$$

Where a = lattice constant, $\lambda = 1.54\text{\AA}$ and θ = Bragg's angle, and hkl are Miller indices. The volume of the spinel unit cell is determined by using the formula:

$$V = a^3 (\text{\AA}^3) \quad (3)$$

The distance between magnetic ions or hopping length is calculated by using the formulae (BABBAR, 1997):

$$L_A = 0.25 a \sqrt{3} \quad (4)$$

$$L_B = 0.25 a \sqrt{2} \quad (5)$$

Where L_A = Hopping length in A-site, L_B = Hopping length in B-site, and ' a ' is lattice constant.

2.1.2. Magnetic Susceptibility

The term magnetic susceptibility (χ) of magnetic materials is defined as the ratio of magnetization (M) to magnetic field intensity (H) (Nikam et al., 2015):

$$\chi = \frac{M}{H} \quad (6)$$

The magnetic susceptibility of ferrites also depends on the temperature, called the Curie-Weiss law. At Curie temperature, ferrites' magnetic susceptibility becomes constant, which is paramagnetic (Callister Jr, 2007).

2.1.3. Construction of Colpitts Oscillator as Susceptometer

The LC oscillator can be used to find the magnetic susceptibility. The tank circuit of LC oscillators consists of two capacitors and an inductor. When the oscillator works, the solenoid's magnetic field is set up. When a magnetic material is put in the solenoid, it gets magnetized. The magnetic field strength is increased, and hence the inductance of the solenoid is increased (Kazimierczuk, 2009; Properties). The frequency of the LC oscillator is determined as (Boylestad & Nashelsky, 2009):

$$f = \frac{1}{2\pi\sqrt{LC}} \quad (7)$$

Since the capacitance (C) is constant, the frequency of LC oscillator is inversely proportional to the square root of inductance:

$$f \propto \frac{1}{\sqrt{L}} \quad (8)$$

The inductance of the solenoid is increased when the ferrite sample is placed in the solenoid field, hence the frequency of LC oscillator is decreased. The circuit diagram for the Colpitts oscillator as susceptometer is shown in Fig.(2). The susceptometer was constructed using the following circuit diagram to measure the magnetic susceptibility.

The tank circuit of the Colpitts oscillator consists of two capacitors and an inductor in the form of a solenoid. The frequency of the Colpitts oscillator is determined as follows:

$$f = \frac{1}{2\pi\sqrt{LC_{eq}}} \quad (9)$$

Where,

$$C_{eq} = \frac{C_1 C_2}{C_1 + C_2} \quad (10)$$

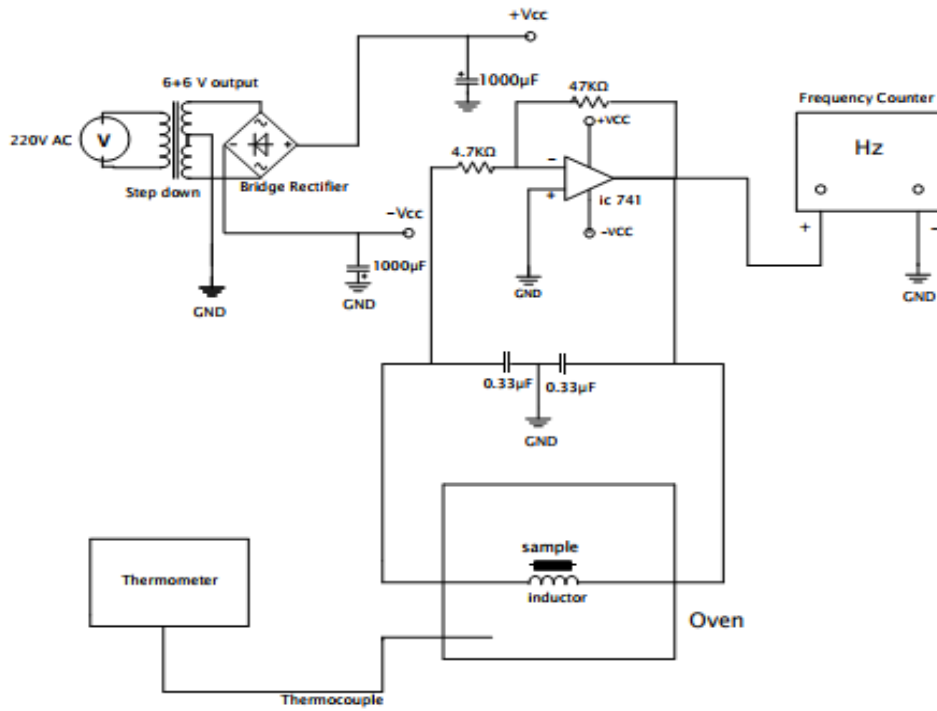


Figure 2: Colpitts Oscillator as Susceptometer circuit diagram

The values of C_1 and C_2 were $0.33\mu\text{F}$, and the solenoid had 550 turns twisted on ceramic paper with copper wire gauge 26 SWG. The length of the solenoid was 5cm, and the volume was 55 cm^3 . The op-amp as inverting amplifier was used for oscillations because the tank circuit provides the 180° phase inversion, and the 180° phase inversion is also provided by inverting amplifier. Thus the total phase inversion is 360° , which satisfies the Barkhausen criterion condition for oscillations. When the sample is inserted into the magnetic field of the solenoid, the frequency changes; this change in frequency was converted into magnetic susceptibility using the following equation (Figueroa et al., 2012; Vannette, 2009):

$$\frac{\Delta f}{f} = -\frac{1}{2} \frac{V_S}{V_C} 4\pi\chi \quad (11)$$

Where f = frequency of oscillator without sample, V_S = volume of sample, V_C = volume of a coil (solenoid), χ = magnetic susceptibility. The Δf changes in the oscillator frequency: $\Delta f = f' - f$, Where f' = oscillator frequency with a sample.

The change in frequency (Δf) with the ferrite sample is negative. This negative sign is canceled with the negative sign of the right-hand side of equation (7); hence the magnetic susceptibility is positive for ferrites. The volume magnetic susceptibility (χ) of spinel ferrites was determined by:

$$\chi = -\frac{2\Delta f}{f} \frac{V_C}{4\pi V_S} \quad (12)$$

The volume magnetic susceptibility (dimensionless) is converted to mass susceptibility (χ_m) as (Cullity & Graham, 2011):

$$\chi_m = \frac{\chi}{\rho} \left(\frac{\text{m}^3}{\text{kg}} \right) \quad (13)$$

$$\chi_m = \frac{\chi}{\rho} X \frac{1000}{4\pi} \left(\frac{\text{cm}^3}{\text{g}} \right) \quad (14)$$

Where ρ = mass/volume = bulk density of the specimen. The mass susceptibility (χ_m) was converted into molar susceptibility (χ_{mol}) as (Raghasudha, Ravinder, & Veerasomaiah, 2013):

$$\chi_{mol} = \chi_m \times \text{Molecular weight} \left(\frac{cm^3}{mol} \right) \quad (15)$$

2.1.4. Dielectric Study

The capacitance and dissipation of spinel ferrite specimens were measured through LCR model 8108 with a frequency range 20 Hz to 1 MHz. The capacitance of the specimen was converted to dielectric constant (ϵ') by using the following formula (Pervaiz & Gul, 2012):

$$\epsilon' = \frac{Ct}{\epsilon_0 A} \quad (16)$$

Where ϵ' = dielectric constant, ϵ_0 = permittivity of free space (8.85×10^{-12} F/m), C = capacitance of the sample, and t = pellet thickness. The dielectric loss was measured from the following equation:

$$\epsilon'' = \epsilon' \tan \delta \quad (17)$$

Where ϵ'' = dielectric loss and $\tan \delta$ = loss tangent.

2.1.5. Resistivity Measurement

The well-known two-probe method was used to find the resistivity of spinel ferrites. For this purpose, the Keithley source meter model 2400 was used. The temperature varied from 300 to 520K during the measurements. The following relation was used to find the resistivity of spinel ferrites (Arshad et al., 2018):

$$\rho = R \frac{A}{t} \quad (18)$$

Where ρ = resistivity of pellet, R = resistance of pellet, A = area of the pellet, and t = thickness of the pellet. The resistance (R) was measured from the slope of the I-V graph.

2.1.6. Activation Energy

The activation energy of spinel ferrites was determined by using the Arrhenius equation given below (Ramarao et al., 2018):

$$\rho = \rho_0 \exp \left(\frac{E_a}{k_B T} \right) \quad (19)$$

Where ρ is the resistivity of spinel ferrite at temperature T, ρ_0 = resistivity of the sample at room temperature, E_a = activation energy, and k_B = 1.38066×10^{-23} J/k (Boltzmann's constant). By solving the equation (17), the activation energy was determined as (Devkunde et al., 2016):

$$E_a = 0.1987 \times \text{slope of the graph (eV)} \quad (20)$$

3. Results and Discussion

3.1. X-ray Diffraction

Fig. 3 shows the XRD patterns of $Co_{0.5}Ni_{0.5}Ti_xFe_{2-x}O_4$ spinel ferrites with $x = 0.0, 0.05, 0.1, 0.15,$ and 0.2 . The XRD analysis of Ti-doped CoNi ferrites prepared by sol-gel auto combustion method and sintered at $1050^\circ C$ for 5 hours revealed the cubic spinel structure. The peaks were identified by comparing the d-values with JCPDS card No. 21-1152. Five peaks characteristic of the fcc structure were observed (220), (311), (400), (422), and (333) with no extra peak that revealed the single-phase cubic spinel structure of Ti-doped CoNi ferrites (Asghar et al., 2018). This is because the Ti is soluble in the lattice, which is substituted in small amounts with interval $x = 0.05$. Since the minute amount of Ti is substituted, no shift in the XRD peaks is observed even though the ionic radius of Ti is larger than Fe. The lattice constant of Ti doped ferrites and unit cell volume are given in Table 1.

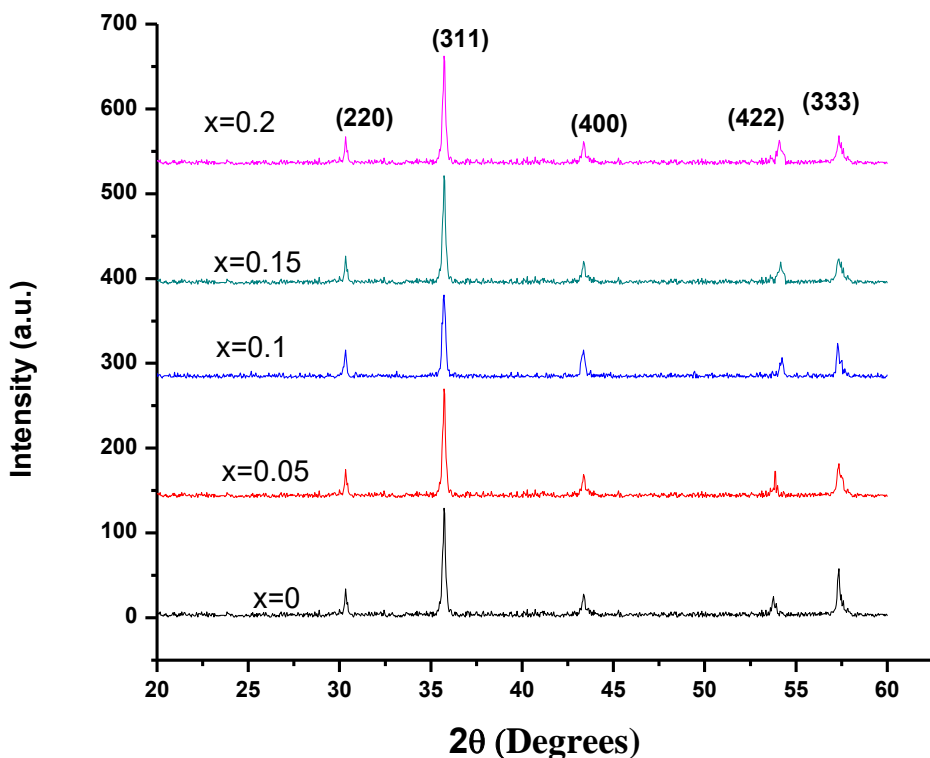


Figure 3: XRD patterns of $\text{Co}_{0.5}\text{Ni}_{0.5}\text{Tl}_x\text{Fe}_{2-x}\text{O}_4$ ($x=0.0-0.2$)

Table 1

XRD parameter of ferrite compositions with varied Thallium content

Thallium content (x)	Ferrite composition	a(Å)	Unit cell volume (Å ³)	L _A (Å)	L _B (Å)
0.0	$\text{Co}_{0.5}\text{Ni}_{0.5}\text{Fe}_2\text{O}_4$	8.223	556.02	3.561	2.907
0.05	$\text{Co}_{0.5}\text{Ni}_{0.5}\text{Fe}_{1.95}\text{Tl}_{0.05}\text{O}_4$	8.235	558.46	3.566	2.911
0.10	$\text{Co}_{0.5}\text{Ni}_{0.5}\text{Fe}_{1.9}\text{Tl}_{0.1}\text{O}_4$	8.245	560.5	3.570	2.915
0.15	$\text{Co}_{0.5}\text{Ni}_{0.5}\text{Fe}_{1.85}\text{Tl}_{0.15}\text{O}_4$	8.258	563.15	3.576	2.919
0.2	$\text{Co}_{0.5}\text{Ni}_{0.5}\text{Fe}_{1.8}\text{Tl}_{0.2}\text{O}_4$	8.269	565.4	3.581	2.923

The lattice constant of Co-Ni ferrites increased from 8.223 to 8.269Å with the doping of Tl^{+3} ions in CoNi ferrites because of the larger ionic radius of the Tl^{+3} ions (1.025Å) than that of Fe^{+3} ions (0.67Å) as shown in Fig (4).

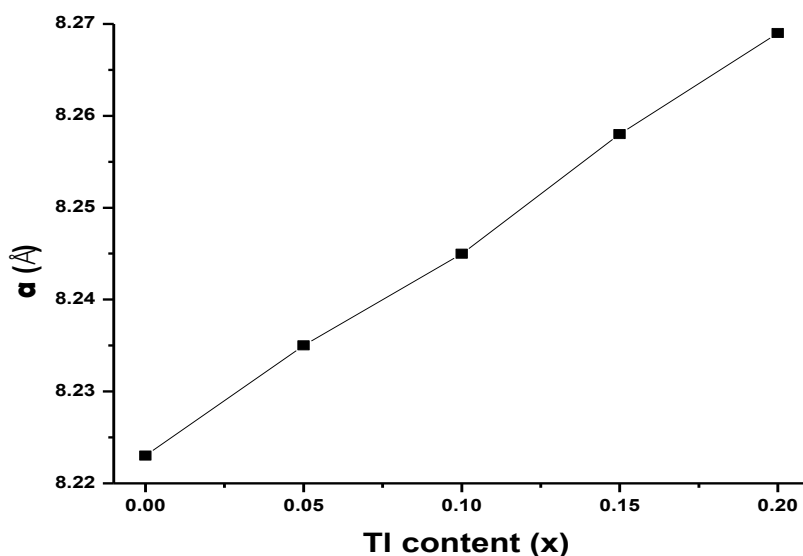


Figure 4: Variation of lattice constant 'a' Vs TI concentration for $\text{Co}_{0.5}\text{Ni}_{0.5}\text{Ti}_x\text{Fe}_{2-x}\text{O}_4$ ($x=0.0-0.2$) ferrites

Lattice constantly followed Vegard's law (Suryanarayana et al., 1998). The hopping lengths LA and LB were calculated using equations (4) and (5) and are listed in Table 1. It is observed that the hopping lengths LA and LB increase due to lattice distortion produced when TI is substituted.

3.2. Magnetic Susceptibility

The temperature-dependent magnetic susceptibility of TI-doped Co-Ni spinel ferrites was determined through the Colpitts oscillator susceptometer at 10 kHz frequency in the temperature range 290-520K. Fig.5 shows the temperature-dependent magnetic susceptibility of TI-doped Co-Ni ferrites. Fig.5 shows that the maximum magnetic susceptibility is $7.46 \times 10^{-3} \text{ cm}^3/\text{g}$ for a sample with $x=0$, and the minimum magnetic susceptibility is for the specimen with $x=0.2$. The magnetic susceptibility continuously decreases with increasing TI contents in ferrite. There are two sublattices in spinel ferrite called A and B-sublattice. Both the sublattices are antiferromagnetically aligned. The total magnetization (M) of spinel ferrites is given by equation (Shinde, 2016):

$$M = M_B - M_A \quad (21)$$

where M_B = magnetization of B-sublattice and M_A = magnetization of A-sublattice.

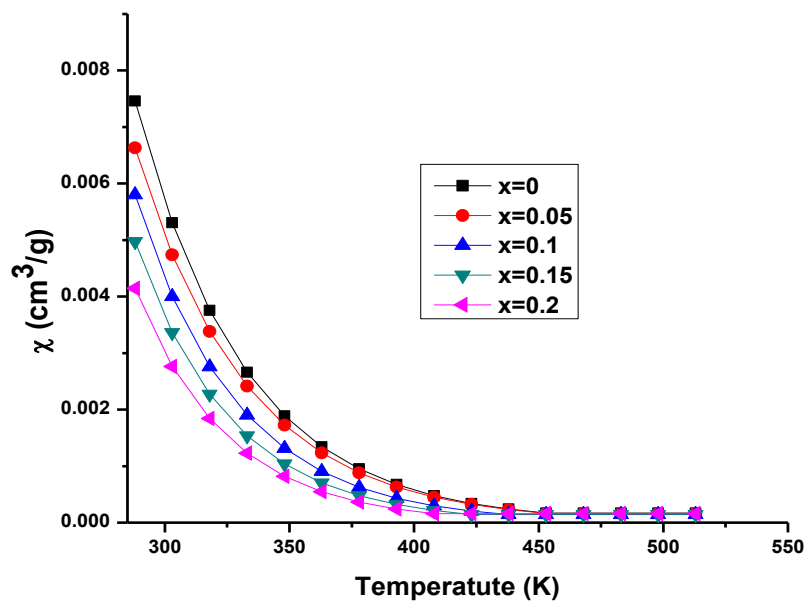


Figure 5: Magnetic susceptibility Vs temperature for $\text{Co}_{0.5}\text{Ni}_{0.5}\text{Ti}_x\text{Fe}_{2-x}\text{O}_4$ ($x=0.0-0.2$)

According to Neel's theory of ferrimagnetism, the A-B interactions are strongest in spinel ferrites than in A-A and B-B interactions. The TI is non-magnetic and prefers B-sites due to its larger ionic radius (1.03\AA) (Goldman, 2006). By increasing the content of Ti^{+3} ions in Co-Ni spinel ferrite the magnetization of B-sublattice (M_B) decreased. Hence the total magnetization (M) is decreased. Thus due to the decrease of magnetization, the magnetic susceptibility is decreased with increasing content of Ti^{+3} ions. The magnetic susceptibility at room temperature, effective magnetic moments, and Curie temperature of ferrite specimens are given in Table 2. The Curie temperature of Co-Ni ferrite decreases with the increasing content of Ti^{+3} ions. The A-B interactions decrease with increasing TI content in CoNi ferrites which causes the decrease in magnetization. Whereas the Curie temperature decreases with TI contents. Fig.5 also shows that the magnetic susceptibility decreases with temperature. At lower temperatures, ferrites' thermal atomic vibrations are small, and the coupling of magnetic forces is large. In ferrites, the magnetic moments are aligned due to coupling magnetic forces. The susceptibility is high at lower temperatures due to large

coupling magnetic forces. When the temperature is increased, the thermal atomic vibrations are increased and dominate the magnetic coupling forces that disturb the alignment of domains in ferrites. Thus the magnetic susceptibility decreases with temperature. The magnetic susceptibility is dropped to a minimum value above Curie temperature. The domains are oriented randomly above Curie temperature and the ferrite sample becomes paramagnetic (Callister Jr, 2007; Kazimierczuk, 2009). Fig.6 (a) & (b) show the plots of TI content Vs magnetic susceptibilities at 300K and Curie temperatures, respectively.

Table 2
Magnetic susceptibility vs temperature content of prepared samples

Composition	χ (cm ³ /g)	Curie Temp. T _c (K)	μ_{eff}	χ_{mol} (cm ³ /mol)
Co _{0.5} Ni _{0.5} Fe ₂ O ₄	7.46X10 ⁻³	453	63.47	1.749
Co _{0.5} Ni _{0.5} Fe _{1.95} Tl _{0.5} O ₄	6.63	450	60.78	1.604
Co _{0.5} Ni _{0.5} Fe _{1.9} Tl _{0.1} O ₄	5.80	438	57.71	1.446
Co _{0.5} Ni _{0.5} Fe _{1.85} Tl _{0.15} O ₄	4.97	423	54.21	1.276
Co _{0.5} Ni _{0.5} Fe _{1.8} Tl _{0.2} O ₄	4.15	408	50.27	1.097

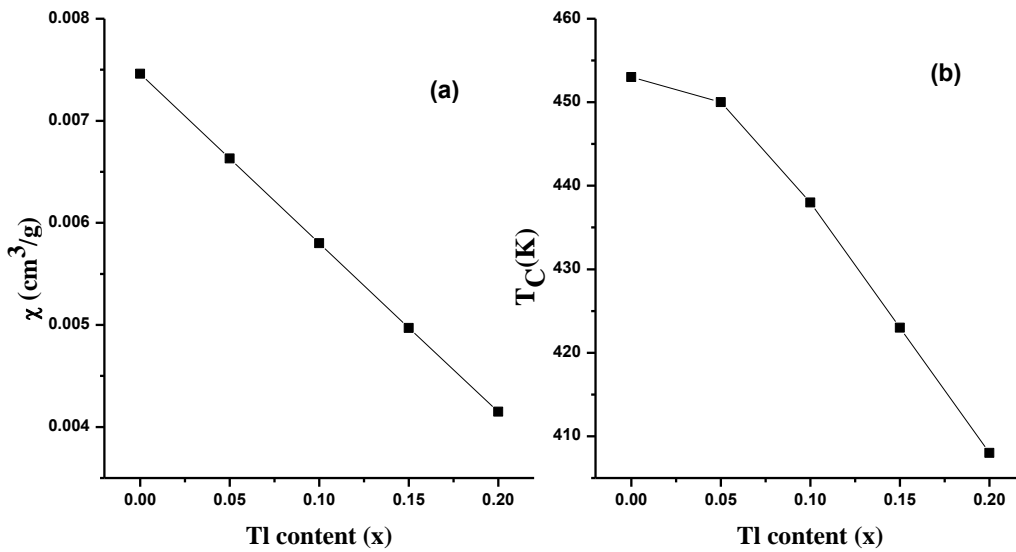


Figure 6: (a) Plot of TI content Vs Magnetic susceptibility at 300K for Co_{0.5}Ni_{0.5}Tl_xFe_{2-x}O₄ (x=0.0-0.2) ferrites (b) Plot of TI content Vs Curie temperature of Co-Ni ferrites

The effective magnetic moment (μ_{eff}) of Co_{0.5}Ni_{0.5}Tl_xFe_{2-x}O₄ (x=0.0-0.2) spinel ferrites was calculated using the following formula [28, 34](Zatsiupa et al., 2014):

$$\mu_{eff} = \sqrt{\frac{3k_B}{N_A \mu_B^2}} X \sqrt{\chi_{mol} T} (\mu_B) \quad (22)$$

$$\mu_{eff} = 2.828 \sqrt{\chi_{mol} T} (\mu_B) \quad (23)$$

Where μ_{eff} = Effective magnetic moment in Bohr magnetrons, k_B = Boltzmann constant (1.38×10^{-16} erg/K), N_A = Avogadro's number (6.022×10^{23}), and μ_B = Bohr magnetron (9.274×10^{-21} erg/G). The effective magnetic moment was observed to decrease with doping non-magnetic (Tl³⁺) ions in Co-Ni spinel ferrites, as listed in Table2.

3.3. Dielectric Constant

The frequency-dependent dielectric properties were determined in the frequency range from 20Hz to 1MHz using equations (16) & (17). Fig.(7a) shows the plot of dielectric constant vs frequency. The dielectric constant (ϵ') and dielectric loss (ϵ'') were observed to decrease with frequency and also observed to decrease with the concentration of Tl³⁺ ions. The interfacial polarization and conductivity of ferrites are due to the presence of Fe³⁺ and Fe²⁺ cations on the B-sites. With increasing the Tl³⁺ ions in Co-Ni ferrites, the content of Fe³⁺ ions decreases on the B-sites because the Tl³⁺ ions prefer B-sites due to their larger

ionic radius. Thus the interfacial polarization is reduced, causing the dielectric constant's value to drop (M. T. Farid, Ahmad, Murtaza, Ali, & Ahmad, 2016).

According to the Maxwell-Wagner model (1951) (Batoo et al., 2009), ferrites consist of two layers; the conducting grains and highly resistive grain boundaries. At lower frequencies, the resistive grain boundaries are more active and resist electrons hopping between Fe^{+2} and Fe^{+3} cations, causing interfacial polarization. At higher frequencies, the conducting grains are more active and allow the hopping of electrons from Fe^{+2} to Fe^{+3} cations; thereby, polarization decreases. Thus, the dielectric constant is decreased at higher frequencies (Batoo et al., 2009; Devmunde et al., 2016). According to Maxwell-Wagner theory, the dielectric loss is also reduced due to decreased space charge polarization, as shown in Fig. (7b).

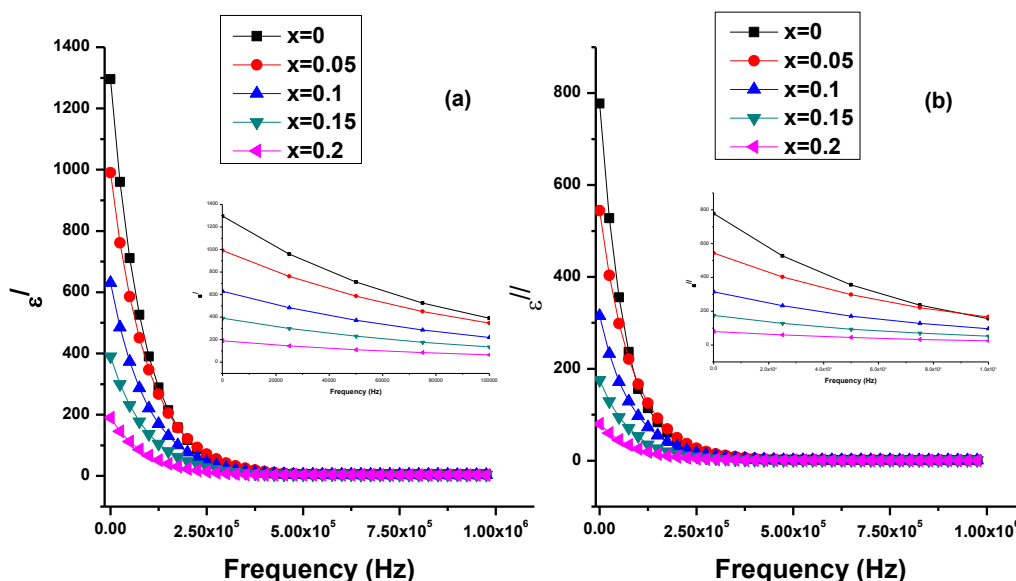


Figure 7: (a) Dielectric constant Vs frequency for TI doped $Co_{0.5}Ni_{0.5}Fe_2O_4$ ferrites (b) Dielectric loss Vs frequency for TI doped $Co_{0.5}Ni_{0.5}Fe_2O_4$ ferrites

3.4. DC Resistivity

Fig. (8) shows the Arrhenius resistivity plots for TI doped $Co_{0.5}Ni_{0.5}Fe_2O_4$ spinel ferrites measured by two probe methods. The resistivity of Co-Ni spinel ferrites was observed to increase with the doping of Ti^{+3} cations (Fig. (9a)).

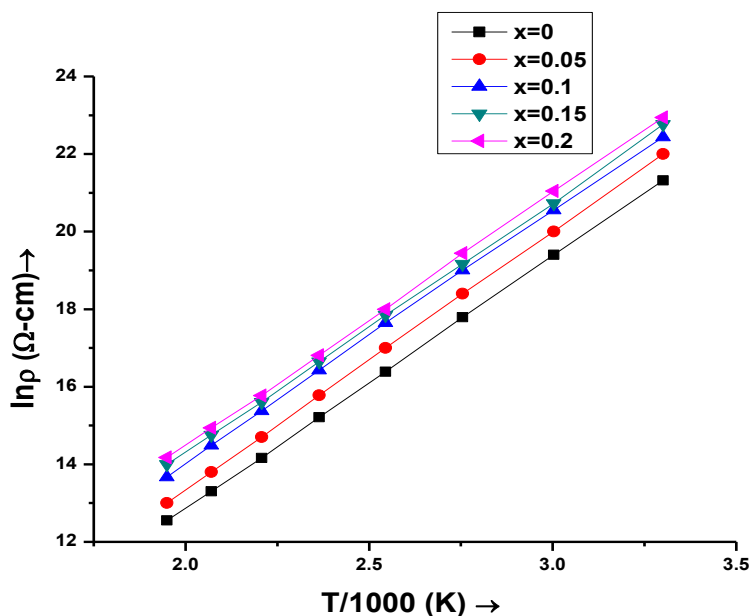


Figure 8: Arrhenius plots for $Co_{0.5}Ni_{0.5}Ti_xFe_{2-x}O_4$ ferrites

According to Verway's mechanism (Arshad et al., 2018), the conductivity of ferrites is due to the presence of Fe^{+2} and Fe^{+3} cations on the B-site. As the Ti^{+3} contents are increased, the concentration of Fe^{+3} cations decrease on the B-sites. The hopping length in B-site (L_B) was found to increase with the doping of Ti^{+3} ions, as mentioned in Table 1. Thus the hopping of electrons between Fe^{+2} and Fe^{+3} cations decreases. So the resistivity of Co-Ni spinel ferrite is increased with doping Ti^{+3} . The resistivity of Ti-doped $\text{Co}_{0.5}\text{Ni}_{0.5}\text{Fe}_2\text{O}_4$ was also observed to decrease with increasing temperature, confirming these ferrites' semiconducting behavior (Bhandare, Jamadar, Pathan, Chougule, & Shaikh, 2011; Pervaiz & Gul, 2012). The activation energy of spinel ferrites was determined from Arrhenius plots as shown in Fig.(9b). The activation energy of Co-Ni spinel ferrite increases with the doping of Ti^{+3} ions according to Verway's hopping mechanism (Devmunde et al., 2016)—the plot of activation energy Vs. Ti contents follow the room temperature resistivity as shown in Fig.(9b).

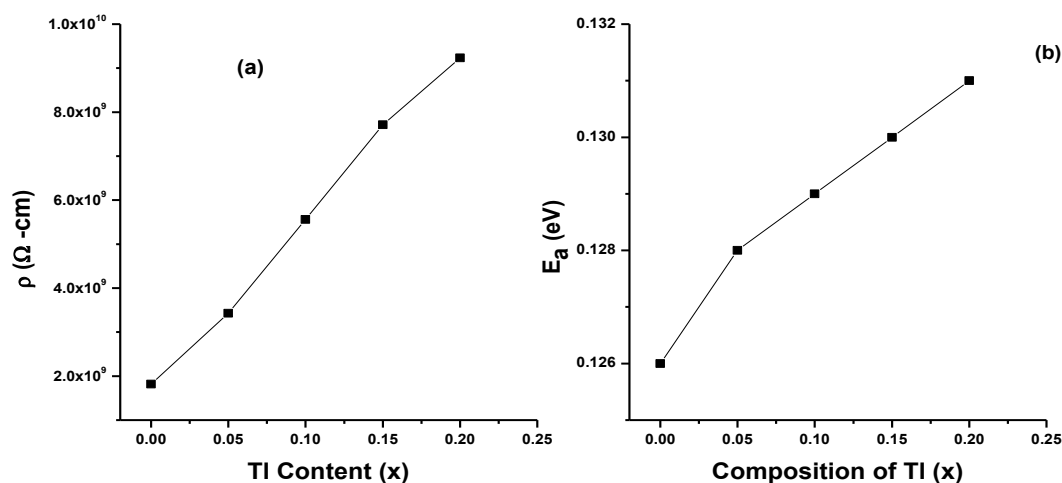


Figure 9: (a) Variation in resistivity Vs TI content for $\text{Co}_{0.5}\text{Ni}_{0.5}\text{Ti}_x\text{Fe}_{2-x}\text{O}_4$ ferrites (b) Plot of activation energy vs TI content for $\text{Co}_{0.5}\text{Ni}_{0.5}\text{Ti}_x\text{Fe}_{2-x}\text{O}_4$ ferrites

Conclusions

The lattice constant was observed to increase from 8.223 to 8.269 Å. The hopping length in the A-sites was found to increase from 3.561 to 3.581 Å, and in the B-sites increased from 2.907 to 2.923 Å with doping Ti^{+3} ions. The magnetic susceptibility at room temperature decreased from 7.46×10^{-3} to $4.15 \times 10^{-3} \text{ cm}^3/\text{g}$, increasing the Ti content from 0 to 0.2. The effective magnetic moment was found to decrease from 63.47 to 50.27 μ_B with doping Ti^{+3} ions in Co-Ni spinel ferrites. The Curie temperature decreases from 453 to 408 K with increasing the Ti contents in Co-Ni ferrites. According to the Maxwell-Wagner model, the dielectric constant and dielectric loss decrease with frequency. The dielectric constant decreases at 20 Hz from 1295 to 190 with increasing the contents of Ti from 0 to 0.2. The dc resistivity of Ti-doped Co-Ni ferrites increases from 1.82×10^9 to $9.23 \times 10^9 \Omega\text{-cm}$ with increasing the contents of Ti from 0 to 0.2. The activation energy was observed to increase from 0.126 to 0.131 eV and follows room temperature resistivity.

Reference

- Abdel-Latif, I. A. (2012). Fabrication of nano-size nickel ferrites for gas sensors applications. *J. Phys*, 1(2), 50-53.
- Abdul-Aziz, A. F., Abraham, A. I., & Khaleel, K. I. (2013). Humidity and Gas Sensitivity of Ni and Co Ferrites pellets with nanoscale grain size at Room Temperature. *Kirkuk University Journal-Scientific Studies*, 8(2), 26-33.
- Amirabadizadeh, A., & Amirabadi, T. (2013). Effect of substitution of Al for Fe on magnetic properties and particle size of Ni-Co nanoferrite.

- Arshad, M., Ikram, S., Mahmood, K., Ali, A., Nabi, A., Amin, N., & Jabeen, F. (2018). Effect of la ions on nickel-cadmium spinel ferrites synthesized by co-precipitation method. *J. Ovonic Res*, 14(1), 27-34.
- Asghar, G., Riaz, M., Khusro, S., Rashid, M., Awan, M., Tariq, G., . . . REHMAN, M. (2018). Effect of Co-Sm substitution on nickel ferrite synthesized by wows sol-gel method. *Journal of Ovonic Research*, 14(4), 317-324.
- BABBAR, V. (1997). *SOLID STATE PHYSICS*: S. Chand Publishing.
- Batoo, K. M., Kumar, S., & Lee, C. G. (2009). Influence of Al doping on electrical properties of Ni-Cd nano ferrites. *Current Applied Physics*, 9(4), 826-832.
- be implemented from June, T. M. Sc. Part-II Chemistry Syllabus as Per New CBCS PATTERN (Inorganic, Organic, Physical and Analytical).
- Bhandare, M., Jamadar, H., Pathan, A., Chougule, B., & Shaikh, A. (2011). Dielectric properties of Cu substituted Ni_{0.5}-xZn_{0.3}Mg_{0.2}Fe₂O₄ ferrites. *Journal of Alloys and Compounds*, 509(6), L113-L118.
- Boylestad, R. L., & Nashelsky, L. (2009). *Electronic devices and circuit theory*: Pearson Education India.
- Callister Jr, W. D. (2007). *Materials science and engineering an introduction*.
- Cullity, B. D., & Graham, C. D. (2011). *Introduction to magnetic materials*: John Wiley & Sons.
- de Almeida, D. A., Junior, E. L. M., da Silva, C. E. S., de Oliveira Pamplona, E., de Oliveira, D. J., Nakagomi, F., & de Freitas, M. R. Projeto Pedagógico do Curso de Engenharia de Materiais Campus Itabira.
- Devkunde, B., Raut, A., Birajdar, S., Shukla, S., Shengule, D., & Jadhav, K. (2016). Structural, electrical, dielectric, and magnetic properties of Cd₂. *Journal of Nanoparticles*, 2016.
- Farid, M., Ahmad, I., Aman, S., Kanwal, M., Murtaza, G., Ali, I., . . . Ishfaq, M. (2015). Structural, electrical and dielectric behavior of Ni_xCo_{1-x}Nd_yFe_{2-y}O₄ nano-ferrites synthesized by sol-gel method. *Digest Journal of Nanomaterials and Biostructures*, 10(1), 265-275.
- Farid, M. T., Ahmad, I., Murtaza, G., Ali, I., & Ahmad, I. (2016). Structural, Electrical and Dielectric Behavior of Ni_xCo_{1-x}Pr_yFe_{2-y}O₄ Nano-Ferrites Synthesized by Sol-Gel Method. *Journal of the Chemical Society of Pakistan*, 38(6).
- Figueroa, A., Bartolomé, J., del Pozo, J. G., Arauzo, A., Guerrero, E., Tellez, P., . . . Garcia, L. (2012). Low temperature radio-frequency transverse susceptibility measurements using a CMOS oscillator circuit. *Journal of Magnetism and Magnetic Materials*, 324(17), 2669-2675.
- Gaffour, A., & Ravinder, D. (2014). Characterization of nano-structured nickel-cobalt ferrites synthesized by citrate-gel auto combustion method. *Int. J. Sci. Eng. Res*, 4, 73-79.
- Goldman, A. (2006). *Modern ferrite technology*: Springer Science & Business Media.
- Jalaiah, K., Mouli, K. C., Krishnaiah, R., Babu, K. V., & Rao, P. S. (2019). The structural, DC resistivity and magnetic properties of Zr and Co co-substituted Ni_{0.5}Zn_{0.5}Fe₂O₄. *Heliyon*, 5(6).
- Kambale, R., Shaikh, P., Kamble, S., & Kolekar, Y. (2009). Effect of cobalt substitution on structural, magnetic and electric properties of nickel ferrite. *Journal of Alloys and Compounds*, 478(1-2), 599-603.
- Kazimierczuk, M. K. (2009). *High-frequency magnetic components*: John Wiley & Sons.
- Kumar, A., Yadav, N., Bhatt, M., Mishra, N. K., Chaudhary, P., & Singh, R. (2015). Sol-gel method, Res. *Journal of Chemical Sciences*, 5, 98-105.
- Nikam, D. S., Jadhav, S. V., Khot, V. M., Bohara, R., Hong, C. K., Mali, S. S., & Pawar, S. (2015). Cation distribution, structural, morphological and magnetic properties of Co_{1-x}Zn_xFe₂O₄ (x= 0-1) nanoparticles. *RSC Advances*, 5(3), 2338-2345.
- Ortiz-Quiñonez, J.-L., Pal, U., & Villanueva, M. S. (2018). Structural, magnetic, and catalytic evaluation of spinel Co, Ni, and Co-Ni ferrite nanoparticles fabricated by low-temperature solution combustion process. *ACS omega*, 3(11), 14986-15001.
- Pervaiz, E., & Gul, I. (2012). Structural, electrical and magnetic studies of Gd³⁺ doped cobalt ferrite nanoparticles. *International Journal of Current Engineering and Technology*, 2(4), 377-387.
- Properties, S. F. Applications EC Snelling. In: Butterworths (edit).
- Raghasudha, M., Ravinder, D., & Veerasomaiah, P. (2013). Effect of Cr Substitution on magnetic properties of Mg nanoferrites synthesized by citrate-gel auto combustion method. *Journal of Chemistry*, 2013.

- Ramarao, K., Babu, B. R., Babu, B. K., Veeraiah, V., Rajasekhar, K., Kumar, B. R., & Latha, B. S. (2018). Enhancement in magnetic and electrical properties of Ni substituted Mg ferrite. *Materials Science-Poland*, 36(4), 644-654.
- Sajjadi, S. P. (2005). Sol-gel process and its application in Nanotechnology. *J. Polym. Eng. Technol*, 13, 38-41.
- Shinde, S. (2016). Crystal structure and magnetic interactions of ferrites. *International Journal of Science and Research*, 5, 1034.
- Singha, A., Singha, J., & Dosanjha, H. (2015). Synthesis of pure and mixed Nickel-Cobalt ferrites ($Ni_{1-x}Co_xFe_2O_4$) by combustion method and characterization. *J. Chem. Pharmaceut. Res.*, 7, 612-617.
- Suryanarayana, C., Norton, M. G., Suryanarayana, C., & Norton, M. G. (1998). *X-rays and Diffraction*: Springer.
- Vannette, M. D. (2009). *Dynamic magnetic susceptibility of systems with long-range magnetic order*: Iowa State University.
- Velhal, N. B., Patil, N. D., Shelke, A. R., Deshpande, N. G., & Puri, V. R. (2015). Structural, dielectric and magnetic properties of nickel substituted cobalt ferrite nanoparticles: Effect of nickel concentration. *AIP Advances*, 5(9).
- Zatsiupa, A., Bashkirov, L., Troyanchuk, I., Petrov, G., Galyas, A., Lobanovsky, L., & Truhanov, S. (2014). Magnetization, magnetic susceptibility, effective magnetic moment of Fe^{3+} ions in $Bi_{25}FeO_{39}$ ferrite. *Journal of Solid State Chemistry*, 212, 147-150.